Three-dimensional Fluid Dynamic Simulation of Radio-frequency Inductively Coupled Thermal Plasmas†

SHIGETA Masaya*

Abstract

This paper presents modelling work and numerical simulations of radio-frequency inductively coupled thermal plasmas (RF-ICTPs) without/with a stationary central injection of a direct-current (DC) plasma jet, which has recently yielded new insights into the three-dimensional structure and dynamics of the plasma flows. The numerical results show that the flows have complicated 3D structures with a noticeable recirculating zone. That recirculating flow prevents the cold sheath gas from flowing downstream through the plasma. The higher-temperature regions in and around the plasma exhibit larger vortex structures principally by the Lorentz force, whereas the lower-temperature flows form smaller eddies by fluid dynamical instability near the top and side walls of the torch. A plasma jet breaks such a structure in the RF coil region, and consequently the flow becomes more complicated. In the RF coil region, the region near the torch wall has a larger standard deviation in the vorticity than the central region.

KEY WORDS: (Plasma fluid dynamics), (Radio-frequency thermal plasma), (3-D modelling)

1. Introduction

Thermal plasma offers a complicated but unique thermofluid field with spatially and temporally varying properties and high enthalpy flows. It has been used as a promising tool for arc welding [1], spray processes [2], waste treatment [3] and nano-material fabrication [4]. Although it is important to understand and control the flow structure for all applications, it is still poorly understood because experiments are generally difficult. Therefore, numerical simulation with mathematical modelling offers a powerful approach to overcome that problem.

In this study, numerical simulations are performed to visualize and clarify the thermofluid field and vortex structure which result from the interactions between argon thermal plasma and cold gas flows. Since most computational studies of thermal plasma flows have used numerically stable but inaccurate schemes, they have never been able to simulate dynamical eddy motions in the thermofluid fields. Meanwhile, the present study has performed more accurate simulations and successfully yielded new insights into the three-dimensional structure and dynamics of radio-frequency inductively coupled thermal plasmas (RF-ICTPs) without/with a stationary central injection of a direct-current (DC) thermal plasma jet [5, 6]. This paper presents the representative results and discussion particularly.

2. Model description

For thermal plasma produced under atmospheric pressure, the local thermodynamic equilibrium assumption is acceptable. It is also assumed that thermal plasma is electrically neutral and optically thin [7]. In addition, the Hall effect is negligible. To treat fluid dynamic motions attributable to multi-scale eddies in and around the plasma, the large grid scale (GS) and the small sub-grid scale (SGS) are separated effectively using a Favre-filtering operation [8]. Hence, the governing equations for the resolved thermofluid field are the Favre-filtered conservation equations of mass, momentum and energy:

$$\frac{\partial \rho}{\partial t} + \nabla \cdot (\rho \boldsymbol{u}) = 0 \tag{1}$$

$$\frac{\partial}{\partial t}(\rho \boldsymbol{u}) + \nabla \cdot (\rho \boldsymbol{u}\boldsymbol{u}) = -\nabla P + \nabla \cdot \boldsymbol{\tau}^{GS} + \nabla \cdot \boldsymbol{\tau}^{SGS} + \rho \boldsymbol{g} \tag{2}$$

$$\frac{\partial}{\partial t}(\rho h) + \nabla \cdot (\rho \boldsymbol{u} h) = \nabla \cdot \left(\frac{\lambda}{C_p} \nabla T \right) - \nabla \cdot \boldsymbol{q}^{SGS} - R + \boldsymbol{S} : \boldsymbol{\tau}^{GS} + \varepsilon^{SGS} \tag{3}$$

where ρ is the density, t is the time, $\boldsymbol{u}$ is the velocity vector, P is the pressure, $\boldsymbol{g}$ is the gravity acceleration vector, h is the enthalpy, λ is the thermal conductivity, C_p is the specific heat at constant pressure, T is the

†Received on June 30, 2014
*Associate Professor

Transactions of JWRI is published by Joining and Welding Research Institute, Osaka University, Ibaraki, Osaka 567-0047, Japan

temperature, $\boldsymbol{q}$ is the heat flux vector, R is the radiation, and ε is the viscous dissipation. The viscosity stress tensor at GS is written as

$$\boldsymbol{\tau}^{GS} = \eta\left[2\boldsymbol{S} - \frac{2}{3}(\nabla\cdot\boldsymbol{u})\boldsymbol{I}\right]. \quad (4)$$

Here, η is the viscosity and $\boldsymbol{I}$ is the unit matrix. The velocity strain tensor is defined as

$$\boldsymbol{S} = \frac{1}{2}\left[(\nabla\boldsymbol{u}) + (\nabla\boldsymbol{u})^T\right]. \quad (5)$$

The superscript T denotes the transpose.

Coupled with the equations of the thermofluid field, the following equation is also solved to determine the vector potential of the induced electromagnetic field:

$$\mu_0\sigma\frac{\partial\boldsymbol{A}}{\partial t} = \nabla^2\boldsymbol{A}. \quad (6)$$

This equation is derived from the Maxwell's equations under the condition of $\nabla\cdot\boldsymbol{A} = 0$. In general, equation (6) incorporates the term of the displacement current in the form of the second derivative of the vector potential with respect to time. However, the magnitude of that term is negligibly small compared with the other terms under typical operating conditions of an RF-ICTP. The electric field and the magnetic field are obtained from the vector potential with the following relations:

$$\boldsymbol{E} = -\frac{\partial\boldsymbol{A}}{\partial t} \quad (7)$$

and

$$\mu_0\boldsymbol{H} = \nabla\times\boldsymbol{A}. \quad (8)$$

The entire flow field, where the plasma at a high temperature and a cold gas at room temperature co-exist, must be treated at the same time. This causes the difficulty of thermal plasma simulations. The widely ranging temperature from 300 to 12,000 K causes large spatial variations of the transport properties with several orders of magnitude. Moreover, the density at a room-temperature region is approximately 45 times that at a high-temperature plasma. Meanwhile, the Mach number is estimated to range from 0.003 to 0.045. Therefore, the partially ionized gas flow is treated as an incompressible flow with the density as a temperature-dependent variable to obtain the solution in a practical time-scale. In addition, it can be conjectured that turbulent and non-turbulent regions co-exist in the flow field because a cold gas has a low kinematic viscosity, whereas a plasma has a high kinematic viscosity. To express this feature, the coherent structure Smagorinsky model [9] is used to estimate the variables at SGS. The more detailed description of the present model is found in Ref. [5] and Ref. [6]. The thermodynamic and transport properties of argon are obtained from Ref. [10] as temperature-dependent data. The data curve of the radiation loss is obtained from Ref. [11].

3. Numerical schemes and computational conditions

The governing equations are discretized by the finite volume method. Because the often-used first-order upwind-differencing scheme cannot capture eddies due to its large numerical viscosity, a central-differencing scheme should be used for the convection terms to capture vortices. However, that scheme easily breaks computation and gives unphysical results. Therefore, in this study, the second-order central-differencing scheme is basically used for the convection terms; however, 10% of the first-order upwind-differencing is blended to stabilize the computation. In addition, the second-order Adams-Bashforth method is applied to time marching.

Figure 1 shows a schematic illustration of an RF-ICTP torch with an additional plasma jet injector. The RF-ICTP is generated with the frequency of 4 MHz by a spiral coil under atmospheric pressure. From the torch top, argon sheath gas (300 K) is injected at 23 sl/min along the cylindrical wall. In addition, an argon thermal plasma jet (12,000 K) is injected at 3 sl/min. The radius of the jet injector is 4 mm. The torch wall is a quartz tube with a diameter of 50 mm and its outside is water-cooled at a constant temperature, 300 K.

Computations were performed by a solver coded in FORTRAN using a supercomputer (SX-9; NEC Corp., Japan) at the Cyberscience Center of Tohoku University.

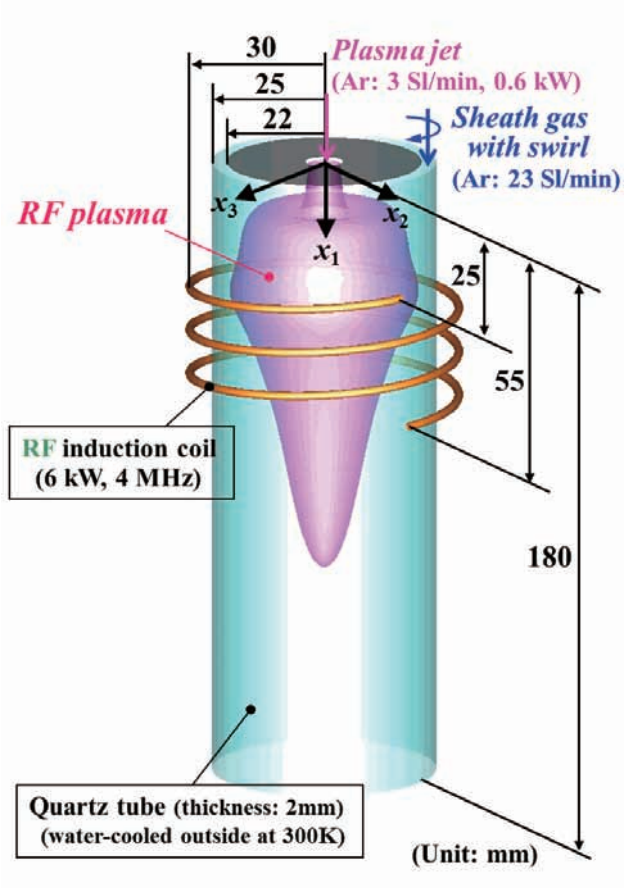

Fig. 1 RF-ICTP torch aided by a DC plasma jet [6].

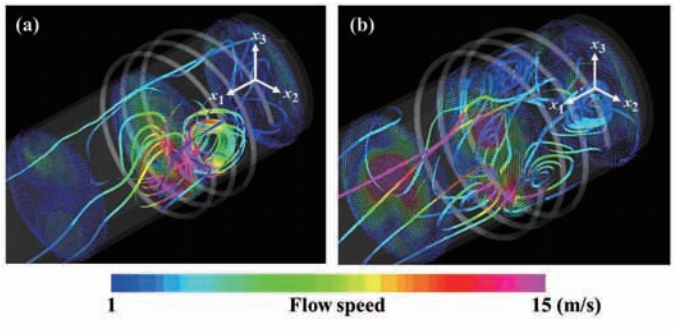

Fig. 2 Flow fields in an RF-ICTP torch: (a) only RF discharge [5], (b) RF discharge combined with a DC plasma jet.

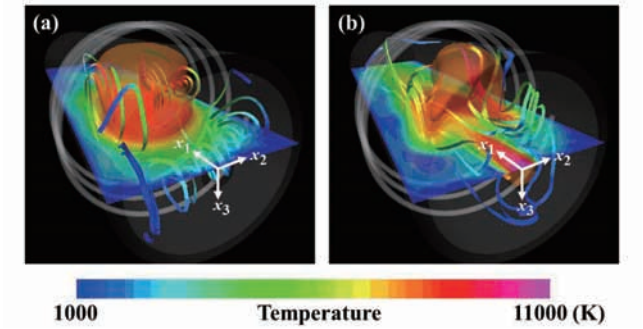

Fig. 3 Thermofluid fields viewed from the torch top [5, 6]: (a) only RF discharge, (b) RF discharge combined with a DC plasma jet. (3D isosurface: 8,500 K).

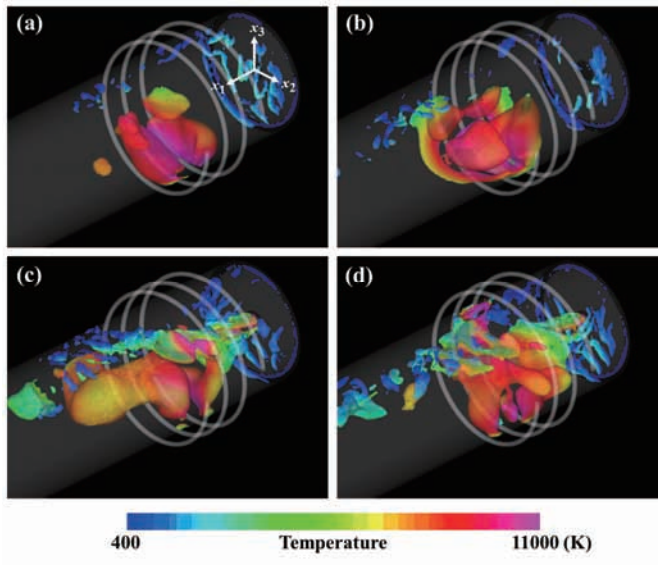

Fig. 4 Vortex structures [6]: (a)(b) only RF discharge, (c)(d) RF discharge combined with a DC plasma jet.

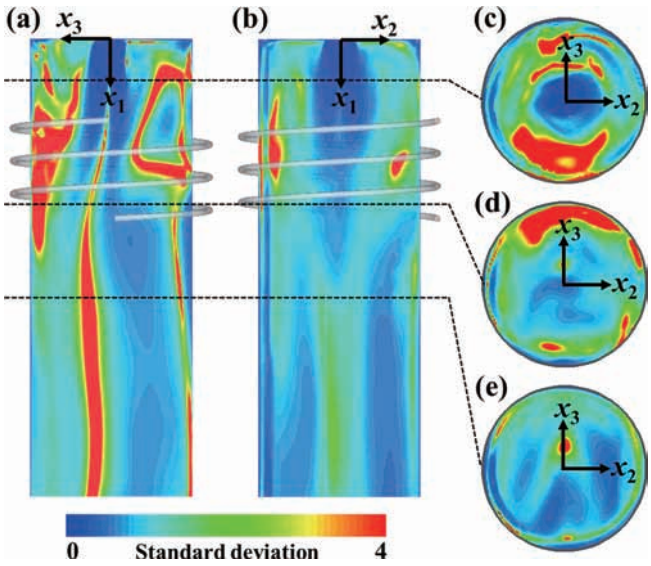

Fig. 5 Standard deviation distributions of vorticity for RF discharge combined with a DC plasma jet.

4. Results and discussion

Figures 2(a) and **2(b)** show the instantaneous flow fields in an RF discharge without and with a DC plasma jet injection, respectively. In both cases, the flows have complicated 3D structures with noticeable recirculating zones. High-speed regions appear where the temperature is high because of thermal expansion. Because a high-temperature plasma has high electrical conductivity, Lorentz forces are generated and drive the fluid motion; consequently, recirculating flows are produced. A DC plasma jet injection causes a more complicated flow structure.

Figures 3(a) and **3(b)** compare typical thermofluid fields when a DC plasma jet is not applied and when it is applied. When a plasma jet is not applied, the larger recirculating flow appears in the plasma and prevents the cold sheath gas from flowing downstream through the plasma. This blocking effect engenders a secondary recirculating flow in the region upstream of the RF coil, as shown in **Fig. 3(a)**. On the other hand, when a plasma jet is applied, the jet breaks such a flow structure as shown in **Fig. 3(b)**.

Figure 4 portrays snapshots of the coherent vortex structures identified with the isosurfaces of the second invariant of the velocity gradient tensor when a plasma jet is not applied (**Figs. 4(a)** and **4(b)**) and when it is applied (**Figs. 4(c)** and **4(d)**). For both cases, the higher-temperature regions in and around the plasma exhibit larger vortex structures, whereas the lower-temperature flows form smaller eddies near the top and side walls of the torch. The high-temperature large vortices are generated and sustained principally by the Lorentz force. Most vortices at a low or intermediate temperature are generated by fluid dynamical instability at interfacial regions having gradients of velocity and density caused by a gradient of temperature at the fringe of a plasma. **Figures 4(c)** and **4(d)** show that the plasma has a much more complex vortex structure because the jet also produces vortices around itself. They interact strongly with the large vortices in the RF coil region.

Figure 5 shows the standard deviations in the magnitude of the vorticity for the RF-ICTP with a DC

plasma jet injection. The zones with large standard deviations are found in the coil region where the plasma behaves dynamically. Especially in the coil region, it is also noticeable that the region near the torch wall has larger standard deviations than the central region.

5. Summary

This study has performed numerical simulations to visualize and clarify the thermofluid field and vortex structure which result from the interactions between argon thermal plasma and cold gas flows. More accurate simulations have been demonstrated, and consequently they successfully yielded new insights into the three-dimensional structure and dynamics of radio-frequency inductively coupled thermal plasmas (RF-ICTPs) without/with a stationary central injection of a direct-current (DC) thermal plasma jet.

Acknowledgments

This work was partly supported by a Japan Society for the Promotion of Science Grant-in-Aid for Scientific Research (C) (Grant No. 23560182). The results of this study were obtained using the supercomputing resources of Cyberscience Center, Tohoku University.

References

[1] M. Tanaka an M. Ushio, Plasma state in free-burning argon arc and its effect on anode heat transfer, *J. Phys. D: Appl. Phys.* **32**, (1999), 1153.

[2] M. I. Boulos, RF Induction Plasma Spraying: State-of-the-Art Review, *Journal of Thermal Spray Technology*, **1**, (1992), 33.

[3] J. Heberlein and A. B. Murphy, Thermal plasma waste treatment, *Journal of Physics D: Applied Physics*, **41**, (2008), 053001.

[4] M. Shigeta and A. B. Murphy, Thermal plasmas for nanofabrication, *Journal of Physics D: Applied Physics*, **44**, (2011), 174025.

[5] M. Shigeta, Time-Dependent 3-D Simulation of an Argon RF Inductively Coupled Thermal Plasma, *Plasma Sources Science and Technology*, **21**, (2012), 055029.

[6] M. Shigeta, Three-dimensional flow dynamics of an argon RF plasma with dc jet assistance: a numerical study, *Journal of Physics D: Applied Physics*, **46**, (2013), 015401.

[7] D. L. Evans and R. S. Tankin, Measurement of Emission and Absorption of Radiation by an Argon Plasma, *Physics of Fluids*, **10**, (1967), 1137.

[8] M. Pino Martín, U. Piomelli and G. V. Candler, Subgrid-Scale Models for Compressible Large-Eddy Simulations, *Theoretical Computational Fluid Dynamics*, **13**, (2000), 361.

[9] H. Kobayashi, The subgrid-scale models based on coherent structures for rotating homogeneous turbulence and turbulent channel flow, *Physics of Fluid*, **17**, (2005), 045104.

[10] M. I. Boulos, P. Fauchais and E. Pfender, *Thermal plasmas Fundamentals and Applications Volume 1*, Plenum Press, (1994).

[11] J. Menart and L. Lin, Numerical study of high-intensity free-burning arc, *Journal of Thermophysics and Heat Transfer*, **12**, (1998), 500.